Stable nonspherical bubble collapse including period doubling in sonoluminescence

Jeppe Seidelin Dam, Mogens T. Levinsen,* and Martin Skogstad
Complexity Laboratory, Niels Bohr Institute, Blegdamsvej 17, DK-2100 Copenhagen Ø, Denmark
(Received 26 August 2002; published 5 February 2003)

We present observations of stable spherical symmetry broken states in single bubble sonoluminescence including observations of period doubled states. States observed involve both spatially oriented states and states with a tumbling symmetry axis. The observations are made using a fiber based four-channel correlation scheme. The measurements are made both with and without narrow band optical filters. The symmetry broken states are seen in all cases even using a 650 ± 40-nm filter. This fact may be used to distinguish between different theories for the light emission. Prior to the measurements reported here, theoretical attempts to explain observations of period doubling bifurcation phenomena in single bubble sonoluminescence were centered on radially bifurcated collapses. The present experiments show unequivocally that the observations are primarily a result of breaking the spherical symmetry in the bubble collapse. Period doubling will at most show up as secondary effects in the total light output, if at all.

DOI: 10.1103/PhysRevE.67.026303 PACS number(s): 78.60.Mq, 47.55.Bx, 47.52.+j

I. INTRODUCTION

Period doubling and chaos are common phenomena in nonlinear systems. Single bubble sonoluminescence (SBSL) [1] represents an extreme example of such systems. It therefore comes as no surprise that shape instabilities and period doubling to chaos have been observed in the system. Here we present evidence that these phenomena in SBSL are linked, giving additional evidence that stable SBSL does not necessarily imply perfect spherical bubble collapse, even if the extinction threshold is linked to the onset of shape distortions.

Sonoluminescence from a single gas bubble levitated in a liquid by ultrasound has been a fascinating subject of recent experimental and theoretical studies [2,3]. For recent thorough reviews we refer to Refs. [4–6]. At high values of the driving sound field the oscillations of the bubble can get sufficiently violent, that in each period the gas in the bubble is compressed to its van der Waals hard core radius. In the process the gas heats up to an extent that leads to light emission [7–12] while the bubble is smallest. In this situation the bubble collapse is highly nonlinear although still mostly thought to be retaining the spherical symmetry, albeit some theories exist that explain the light emission in terms of symmetry breaking (jets, etc.) [13]. In fact, the boundary of stability was for a long while commonly believed to coincide with the loss of spherical symmetry.

The original experiments on single bubbles reported a synchronicity with the driving sound field (typically ≈ 27 kHz) on the order of 50 ps, thus showing a remarkably stable dynamics (Barber *et al.* [14]. Later, several authors reported various kinds of observations of period doubling [15–17], quasiperiodicity, and chaos [15]. However, all these observations were done with a single photomultiplier, and the underlying mechanism responsible for the observed behavior has not yet been identified.

The first experimental evidence that a single isolated light emitting bubble could collapse into a nonspherical state, was obtained by Weninger *et al.* [18] using a two point angular correlation setup. This suggested that a distorted state with random orientation (presumably an $n=2$ spherical harmonic state) could be excited, since the far field intensity distribution of the emitted light had a dipolar component. This observation was tentatively explained by refraction of the light from a central emitter at the bubble surface [18,19]. Shape instabilities were observed directly for larger nonsonoluminescent bubbles by Tian *et al.* [20] using a photographic method (see also Trinh *et al.* [21]), and inferred for smaller sonoluminescent bubbles from bubble stability measurements compared to theoretical predictions of the position in parameter space of the shape instability boundary [17,22]. These measurements were interpreted as showing that stable nonspherical sonoluminescent bubbles were observed below the $n=4$ shape instability boundary but above the $n=2$ shape instability boundary. On the other hand, new theoretical calculations [23–26] find that the instability is overestimated, voiding this interpretation.

However, recently an angular correlation experiment showed conclusively that SBSL with period doubled light emitting states involved shape distortions [27] on a stable bubble.

Early attempts to explain period doubling in multibubble sonoluminescence and SBSL centered on spherically symmetric collapse [15,28–30]. A detailed study on SBSL based on the Rayleigh-Plesset equation [31–33] was performed by Simon *et al.* [34]. This study showed that the parameter space for period doubling is far from that, where light emission takes place, if only radial dynamics is considered. Also found here was that a memory effect involving the afterbounces was involved in these models in catalyzing the instabilities. In the regime of SBSL the afterbounces die out long before the next collapse and thus can hardly be the cause of the necessary memory. A suggestion in the latter paper pointed to the returning echo of the bubble collapse as a possible mechanism for a feedback (see also Ref. [35]).

However, as said above, these different model calculations all assume that the bubble collapse preserves the

*Electronic address: levinsen@nbi.dk

spherical symmetry, i.e., the bifurcations are solely due to a size effect. In our fiber based four-channel correlation measurements on SBSL presented here, contrary to this assumption, we find that instabilities leading to pulse height period doubling are always associated with a spontaneous break in the spherical symmetry of the collapse and will at most show up as secondary effects in the spatially integrated light output per flash, if at all.

This suggests the possibility of a parametric excitation of a shape distortion, the growth of which is limited by nonlinear effects. Period doubling in this picture is then due to a secondary instability in the governing Hill equation for the shape distortion and thus does not need any further feedback mechanism of the type described above.

The paper is organized as follows. In Sec. II we shall describe the experimental setup. In Sec. III we first give some general information on the data analysis, then treat results, obtained through measurements performed with narrow optical filtering, that can only be interpreted as arising from breaking the spherical symmetry. This is followed by a discussion on how to interpret time series and the relevance of the autocorrelations versus cross correlations. Here we will show examples of states of spherical symmetry and distorted states. Next to be discussed are the spatial symmetries involved, and finally correlations over long offset times, and the analysis of oscillations in these. In Sec. IV we shall first discuss period doubling with short time correlations and then period doubled states with a preferred symmetry direction in space. Section V deals with the possible theoretical perspectives of the outcome of the experiments and finally in Sec. VI we sum up the experimental results and our conclusions.

II. THE FOUR-CHANNEL CORRELATION EXPERIMENT

The vessel used is a glass sphere of 6.5-cm diameter and wall thickness ~ 0.25 mm hanging acoustically isolated in its neck tube of 7-mm inner diameter. A pair of piezoelectric transducers is glued on to opposite sides with epoxy. The drive signal of approximately 25 100 Hz is delivered by a computer controlled HP 33120A function generator, through a power amplifier and tuning circuit. The flask is filled with outgassed distilled water and placed in a modified refrigerator. After cooling to a temperature of approximately 5 °C and allowing for temperature equilibrium to be reached, a bubble is generated by a computer controlled blast of air on the free surface. The computer is programmed to automatically redo this, if bubble extinction occurs (or none is generated), and also automatically search for stable light emission above a preset intensity limit.

The correlation setup consists of four quartz fibers of 1-mm diameter leading the emitted light to four photomultiplier tubes (PMTs) (Hamamatsu H5783P-03, risetime 0.65 ns). The fibers are placed at well defined longitudes in the equatorial plane of the sphere pointing at the bubble from a distance of ~ 4.5 cm. For an overview of the setup see Fig. 1. Using four fibers allow for a simultaneous measurement of correlations involving six angles, thus creating a comprehensive spatial knowledge simultaneously for all these angles. The signals from the PMTs are amplified by preamplifiers

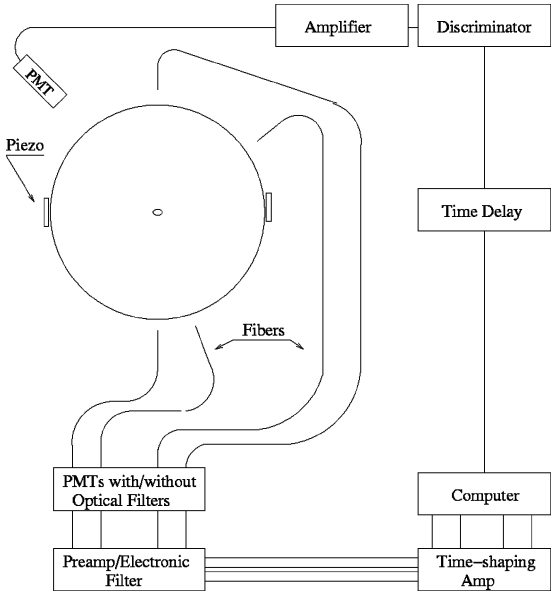

FIG. 1. Overview of the correlation setup.

and time-shaping amplifiers (shaping time 3 μs), and fed to a 20-MHz four-channel simultaneously digitizing analog-to-digital (*A-D*) data acquisition card (ADLink 9810). A fifth photomultiplier tube that looks directly at the bubble provides the digitizer timing signal, which is delayed so that the *A-D* card measures the peak value of the pulse. The reliability of the trigger system has been carefully checked to ensure exactly one sampling per flash. The peak value of the pulse observed in each of the four channels (CH0, CH1, CH2, CH3) for every flash is recorded in time series of length 3×10^6 flashes (≈ 2 min). To avoid cross talk between channels, all PMTs and amplifiers have separate power supplies and the performance of the system has been carefully checked in trial runs.

Interference phenomena play an important role in the interpretation of the correlation experiment. An important parameter of the detection system is therefore its overall frequency response including the absorption in the wall of the glass sphere, folded with the expected spectrum of the emission from the bubble. This is displayed in Fig. 2. As seen, the dominant contribution to the pulse heights measured without additional optical filtering (used in some single photon measurements to be discussed) comes from the region of 280–450 nm.

III. EXPERIMENTAL RESULTS

A. General remarks

The time series obtained in this fashion seem rather confused at first glance. This is mostly due to the small number of photons (notice that pulse height, proportional to $\hbar\omega$, depends on the wavelength of the detected photon) detected from a single pulse as the solid angle seen by the bubble is very small, but also due to the statistical nature of the PMT detection process (see also discussion below). Apart from long time oscillations of frequencies around a few Hertz, the output is stable and the bubble can survive for many hours

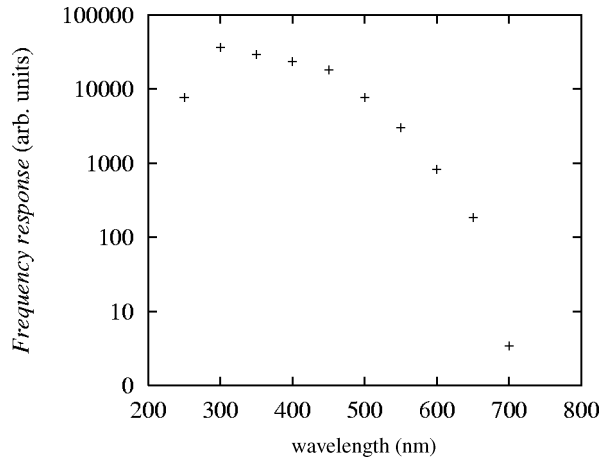

FIG. 2. Frequency response of the detection system folded with the spectrum of the emission from the bubble.

without extinction. A sliding point average (of order 100 points or more) is often necessary before features like, e.g., period doubling are clearly discerned. Note that to see period doubling requires dividing the time series into two and treating the measured pulse heights at odd and even times (measured in units of the sampling interval $T=1/\nu$, ν being the frequency of the driving ultrasound) separately. The time series are scanned for abrupt changes or indications of period doubling. Tracks showing these features are treated separately.

As will become evident in the following, operating the bubble close to the extinction threshold and allowing for a gradual change by diffusion of the amount of dissolved gases results in scanning through a parameter space, where the bubble often develops stable shape oscillations and even may experience periodic shifts between different states with broken spherical symmetry (period doubling). For each choice of spatial configuration of fiber positions, the average output of each channel is calculated for the entire body of time series involved (often a total of several days). As no states of preferred direction in space can be expected to last this long, the average can be taken a calibration of relative interchannel sensitivities, and deviations observed in individual time series taken as indicating a symmetry broken state.

While information gleaned this way can often be used to analyze states of preferred spatial orientations with and without period doubling, statistical methods have to be invoked to analyze states that are either short lived or without a preferential spatial direction. One way to analyze the spatial and temporal properties of such states is to calculate autocorrelations and cross correlations as function of offset time (a precise definition is to be given below).

The use of four detectors gives the possibility of simultaneously obtaining cross correlations involving six angles. The measurements involve settings with all fibers in the horizontal plane (either distributed over 90° or over 180°) and some with one fiber placed directly below the bubble and the rest still in the horizontal plane. Measurements were furthermore performed without filtering, with blue filters, with red filters, and with a combination of blue and red filtering.

An open system was chosen since this automatically let us to scan a much larger parameter space due to diffusion than a sealed system would allow us. The content of dissolved air is 20% at the start of the run and approximately 30% air at the end.

From the measurements of the spatial distribution of the intensity of the emitted light, one would naturally hope to be able to extract information on the shape of the bubble and on the physical state inside the bubble at the time of emission, as well as on the mechanism behind the light emission itself. The angular dependence found in the measurements by Weninger *et al.* [18] using a two point angular correlation setup, suggested that a shape distorted state with random orientation could be excited. This observation was tentatively explained by refraction at the surface of a nonspherical bubble of the light from a central emitter [18,19] with most of the interior being nearly transparent for the radiation [36]. However, other models exist where the radiation is supposed to be mostly from the surface [37–41]. The model described in Ref. [41] was explicitly set up to explain the dipolar radiation term in the intensity. Unfortunately, no results for the spatial correlation based on these different models have been obtained so far. Be this as it is, important information that could allow to distinguish between the different models is clearly hidden in the change of the spatial distribution observed when different wavelength intervals are investigated.

B. Narrow optical filter results

In the measurements by Weninger *et al.* [18], the investigation of the wavelength dependence was performed with comparatively broadband filters (''blue'' filter 280–320 nm, ''red'' filter >500 nm) and a dipolar state was observed using the ''blue'' filter. However, using the ''red'' filter, the size of the effect was seemingly much smaller and hidden in the noise if at all present.

We have performed similar measurements but with filters of comparatively narrower range (''blue'' 405 ± 5 nm, ''red'' 650 ± 40 nm). With such narrow filters the measurement becomes a single photon correlation measurement with an average photon count per channel varying from $\sim1\%$ for the red filter to $\sim10\%$ per flash for the blue filter. (For the present purpose there is no need to make corrections for the statistical probability of two photon detection.)

Theoretically, the time dependent correlations in the single photon case are defined by

$$C_{k,l}(t)=\frac{P_2(k,l,t)}{P_1(k)P_1(l)}, \tag{1}$$

where $P_2(k,l,t)$ is the joint probability to measure a photon in both CHk and CHl with time difference t, while $P_1(k)$ and $P_1(l)$ are the probabilities to measure a photon in CHk and CHl, respectively, with $(k,l\in\{0,1,2,3\})$. Here CHk and CHl are the two channels over which the correlation is being calculated with $k=l$ giving the autocorrelations and $k\neq l$ the cross correlations. Furthermore, t is the offset time in units of sampling interval.

However, if a slow drift in the average intensity is present,

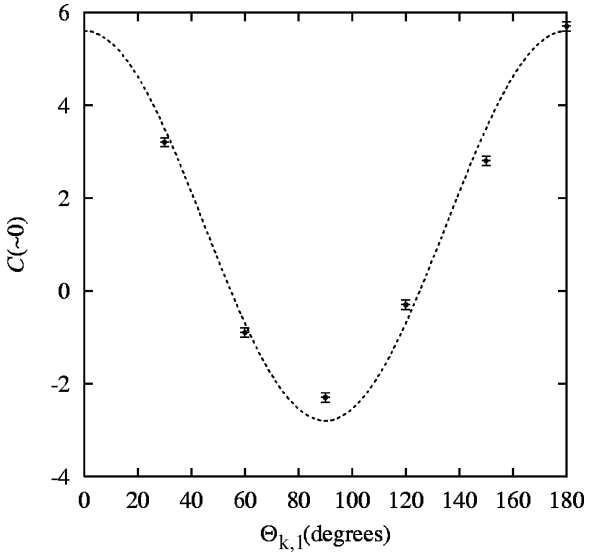

FIG. 3. The weighted mean value of $C(t)$ (parts per thousand) for $t=2$ to 20 plotted as a function of angle for a 90-h run with blue filters (405 ± 5 nm) inserted. The dashed line is $0.001\,40[1+3\cos(2\Theta_{k,l})]$.

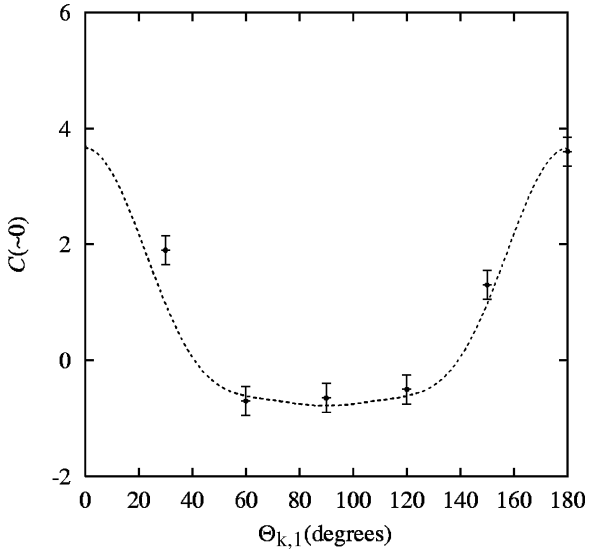

FIG. 4. The weighted mean value of $C(t)$ (parts per thousand) for $t=2$ to 20 plotted as a function of angle for a 400-h run with red filters (650 ± 40 nm) inserted. The dashed line is $0.000\,55[1+3\,cos(2\Theta_{k,l})]+0.00045\cos(4\Theta_{k,l})[2+\cos(2\Theta_{k,l})]$.

the above definition is not practical. Instead we use the following definition:

$$C_{k,l}(t,t_2)=\frac{C_{k,l}(t)}{C_{k,l}(t_2)}-1=\frac{P_2(k,l,t)}{P_2(k,l,t_2)}-1\sim\frac{N(k,l,t)}{N(k,l,t_2)}-1, \tag{2}$$

where $P_2(k,l,t)$ and $P_2(k,l,t_2)$ as above are the joint probabilities to measure a photon in both CHk and CHl with time difference t and t_2, respectively. $N(k,l,t)$ and $N(k,l,t_2)$ are the total number of counts of photon pairs in CHk and CHl with time difference t and t_2, respectively. Here $t\ll t_2\ll N$ where N is the total number of sampling times. This effectively normalizes the correlation such that the long time behavior that is believed to be uncorrelated falls together for all cross correlations belonging to the time series under investigation. In the following we shall omit t_2 for simplicity.

Because of the small number of photons detected in a single photon experiment, the measurement has to run for a prolonged period in order to get sufficiently good statistics. With an open system this means averaging over many different runs where the water has been outgassed anew.

In Fig. 3 we present the result of a 90-h run plotting the angular dependence of the cross correlation averaged over the first few offset times ($t\sim0$). Over this prolonged period of time one would expect all effects of preferred directions in space to be washed out. The fibers are placed in the horizontal plane such that channel and angle correspondence is CH0, 0°, CH1, 30°, CH2, 120°, and CH3, 180°.

The far field intensity distribution of the emitted light, if point symmetric (no significant deviations from this has been observed), can be written in a multipole expansion. For a spherical bubble collapse this expansion would of course only contain a monopole term. However, as in the case of Weninger *et al.* [18], we need to include a dipole term to fit the experimental data. The contribution of such a term to the cross correlation is given by

$$C_{k,l}(0)=\frac{N_D^2}{(N_I+N_D)^2}\left(\frac{1}{5}+\frac{3}{5}\cos2\Theta_{k,l}\right). \tag{3}$$

Here N_I represents the photons emitted isotropically in the solid angle of the detectors and N_D those emitted as from a dipole. Furthermore we have assumed that there is no preferred direction to the dipole over the time of the data collection. The fit is, as in their case, quite convincing. As already pointed out in Ref. [18], this angular dependence cannot be explained by a spherically symmetric collapse, even with a fluctuating output per glimpse, since all observers (fibers) in this case would see the fluctuations as being in phase. Movement in space will also affect correlations but if one observer sees photons more often as the bubble moves towards him, the observer 180° off will see less photons as the bubble moves away. The cross correlation will therefore be symmetric around 180° and not around 90° as observed.

A similar plot for a 400-h run with the red filters (same position of fibers) is presented in Fig. 4. Since the spectrum of the light is much weaker and the quantum efficiency of the detector much less in the red than in the blue, we need much longer time series to obtain acceptable statistics.

A fit to the experimental data in Fig. 4 seems to indicate the additional presence of a quadrupolar component,

$$C_{k,l}(0)\propto\cos(4\Theta_{k,l})[2+\cos(2\Theta_{k,l})]. \tag{4}$$

We should add here that the relative change between cross correlations for different angles is determined with smaller uncertainty than is the absolute zero level (which depends on the choice of t_2 in the definition of the correlation). More astonishing is that there is no great difference between the

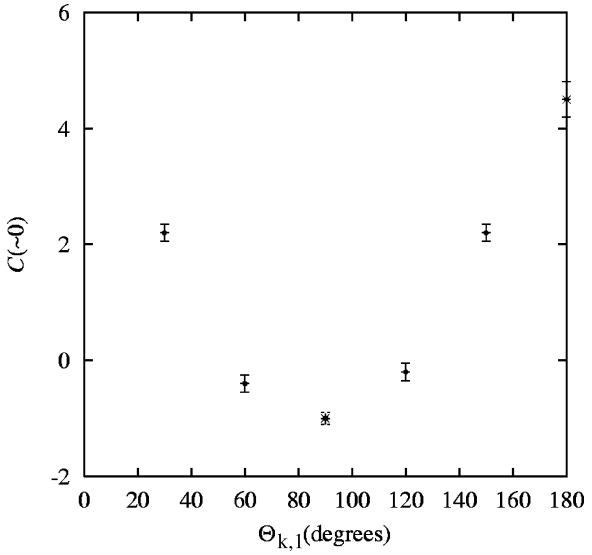

FIG. 5. The weighted mean value of $\Delta C(t)$ (parts per thousand) for $t=2$ to 20 plotted as a function of angle for a 186-h run with two channels having blue filters (405 ± 5 nm) inserted and two channels having red filters (650 ± 40 nm). The point at 180° corresponds to red-red channel correlation while that at 90° corresponds to blue-blue and the rest are mixed.

absolute size of the change with angle for the cross correlations in the two different filter cases. Of course, since the measurements do not coincide in time, this may simply be a result of the bubble on the average being distorted much more in the case of the red filters.

In order to get a better understanding, we have also performed a measurement with two red and two blue filters. The result of a 186-h measurement with this combination is presented in Fig. 5.

Even though a quantitative comparison cannot be performed, since the nature of the state behind is unknown, it is evident from these graphs that the wavelength dependence is not nearly as strong in our case, as one would have guessed from the measurements of Weninger *et al.* [18]. While there probably is a dependence on wavelength, the effect certainly does not disappear for ''red light.'' This could be due to the bubble size being different in the two experiments with ours being the larger (due to, e.g., lower temperature, higher air concentration, etc.), that they average over a larger region of wavelength, or simply that noise is disguising the angular dependence for the ''red'' light in their experiment.

With regard to the actual bubble size in our experiment it was impractical to make this measurement in the present setup. However, from other experiments under similar conditions where the bubble size was measured by a new technique (calibrated against Mie scattering) [42], we can estimate the ambient bubble radius R_0 to be around 6 μm and $P_A\sim1.45$ bar when shape distortions are present.

We shall see below whether or not one is able to deduce something about the actual physical state from this type of measurements. It suffices to say here that the existence of a quadrupolar emission component by no means implies a more complicated geometrical state than an $n=2$ state, at least if interference effects are present. For the same reasons, it does not mean that the bubble observed in the ''red'' was more distorted than the bubble observed in the ''blue,'' since interference effects are critically dependent on the actual bubble size. In the theoretical explanation given in Ref. [19] the light is assumed to be emitted from the center region of the bubble. The light is then diffracted at the bubble surface and the resulting far field light intensity can be described by a multipole expansion due to the interference of light coming from different surface segments of the bubble. For a spherically symmetric bubble only the monopole contribution is present. However, even for an ellipsoidal shape higher-order terms will be needed, the relative strength of the components depending on parameters such as wavelength, bubble size, degree of ellipticity, relative refractive indices, etc.

C. Spherical and distorted states

In the following section we shall describe measurements performed without filters inserted in front of the PMT's. This has the advantage that much shorter datafiles are needed to obtain the necessary statistical accuracy. Thus states with short lived shape oscillations, distorted states of preferred spatial orientations, states that are period doubled in flash strength, and even transient states [43] can be investigated. The price paid is that the wavelength dependence is somewhat smeared out (see Fig. 2).

As was the case for Weninger *et al.* [18], we apparently find states both with and without multipole components present in the spatial distribution of the emission. However, we also found states that were obviously period doubled. All these states were long lived in the sense of surviving for minutes or more, but mostly the bubble progressed from one such state to another, thus surviving for many hours, probably due to the change in the contents of dissolved gases brought about by diffusion since the system is open.

In Fig. 6 we show a 120-s-long time series with a 600-ms sliding point average. The first part displays a ''fluctuating'' emission signal with comparatively large excursions from average in all channels while the second part shows a much more ''quiet'' signal in all channels with a change from one state to the other in the middle of the time series. The flash intensity goes to zero in this region for a very short time. However, the bubble is not lost completely but gradually recovers. The configuration used is CH0, 0°; CH1, 15°; CH2, 60°; CH3, 90°. In this plot as in all that follows, we have normalized with the average signal for the channel in question taken over the entire sequence for the configuration (in this case 47 h).

The distribution of signal strength for CH0 is displayed in Fig. 7 for the two cases. As expected, the distribution corresponding to the ''quiet'' part is narrow while that corresponding to the ''fluctuating'' part is broad. The information in the two time series is high enough, that the cross correlations can be calculated with a reasonably small degree of uncertainty. Here the autocorrelations and cross correlations are defined by

$$C_{k,l}(t)=\frac{\Sigma_{m=1}^{N}[Q_k(m)-\overline{Q_k}][Q_l(m+t)-\overline{Q_l}]}{N\overline{Q_kQ_l}}, \qquad (5)$$

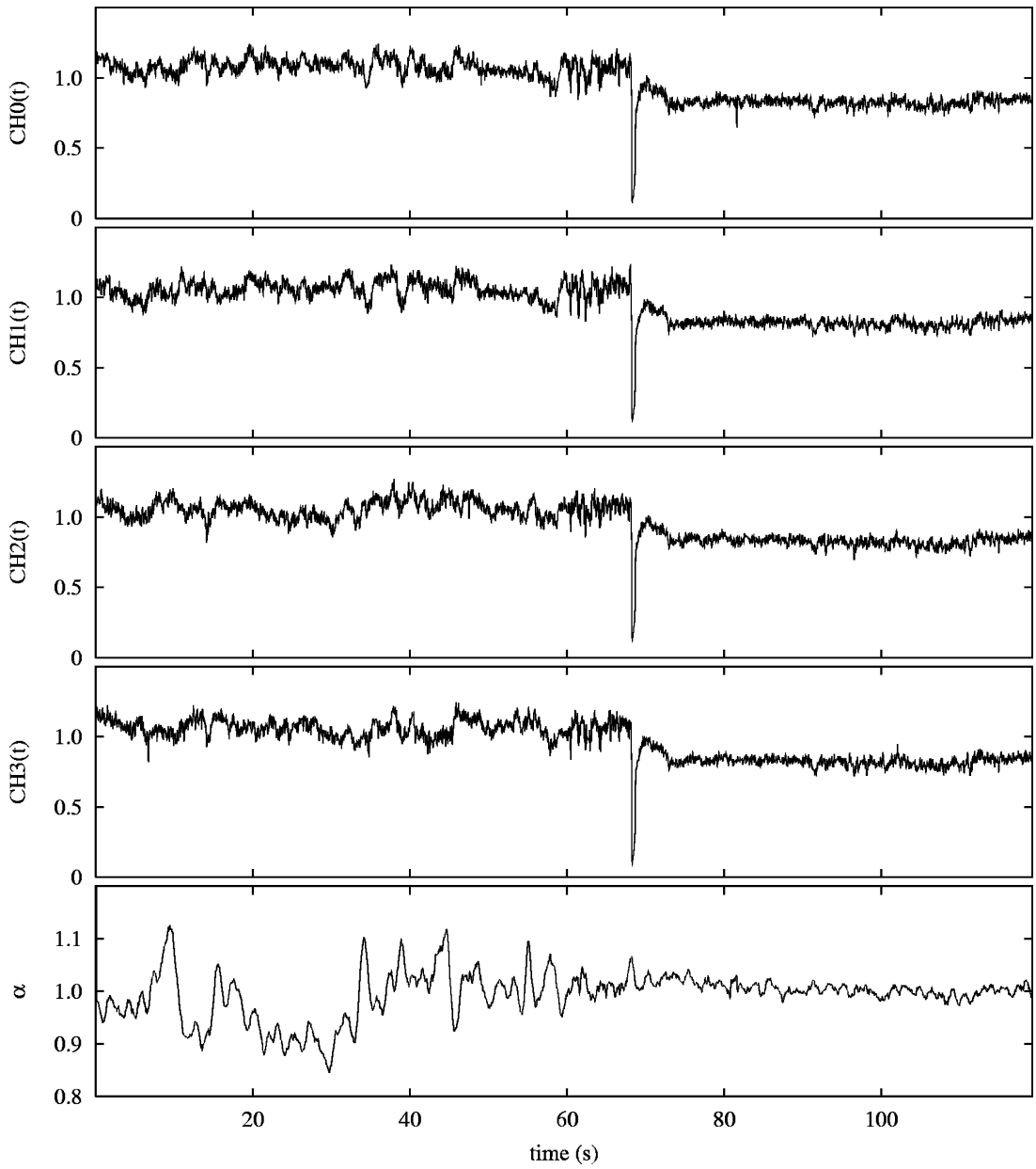

FIG. 6. Time series showing a noisy signal in all four channels, which after the light emission collapses (without the bubble disappearing completely) turns into a quiet signal in all channels. The signals have undergone a sliding point average corresponding to 600-ms binning to remove the statistical noise arising from the small count numbers per flash. Please note that the ratio α between the intensities of channels CH2 and CH0 is also plotted in order to elucidate the change to an isotropic intensity distribution.

where N is the total number of samples in the time series for the two channels CHk and CHl ($k,l \in \{0,1,2,3\}$) over which the correlation is being calculated with $k=l$ giving the autocorrelations and $k \neq l$ the cross correlations. Here m denotes a specific sample and $t \ll N$ the offset time in units of sampling interval. $Q_h(m)$ is the signal size in CHh at time m and $\overline{Q_h}$ is the signal size in CHh averaged over all samples in the (usually 2-min long) time series being investigated. For the autocorrelations ($k=l$) t is always positive while for the cross correlations ($k \neq l$) all t's are allowed. Unless otherwise specified, the cross correlation $C(t)$ denotes average value of $C(t)$ and $C(-t)$.

Notice that for a given offset time, higher than average signals in both channels or lower than average signals in both channels give rise to positive contributions. Higher than average in one channel together with lower than average in the other channel give a negative contribution to the cross correlation.

In the case of the data from the ''quiet'' part, there seems to be no angular dependence for the cross correlation, while in the case of the data from the ''fluctuating'' part, the angular dependence looks similar to that found with the ''red'' filter although the amount of quadrupole content is even higher (see Fig. 8). A similar result was found by Weninger *et al.*, but no explanation offered, although it was noted that the jitter in the timing of the flashes was surprisingly identi-

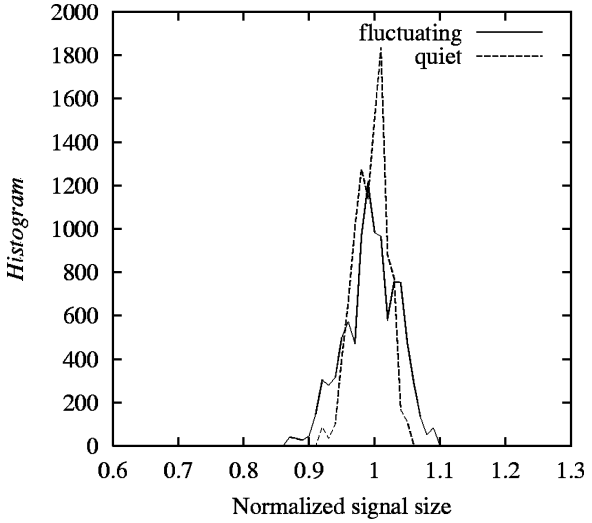

FIG. 7. The signal strength distribution belonging to CH0 of the time series displayed above in Fig. 6 using the same sliding point average of 20 ms to remove the statistical noise from the small count numbers per flash as above. The broad distribution is from the first ''fluctuating'' part while the more narrow distribution is from the later ''quiet'' part.

cal in the two cases. This led to the conclusion that the state with dipolar radiation content could not be connected to the chaotic states observed in Ref. [15].

The estimate of the average strength in a given channel obtained by averaging over the entire time series of the configuration investigated can, however, in some cases offer some enlightenment of the situation. In the lower part of Fig. 6 is displayed the ratio α between the intensities measured in

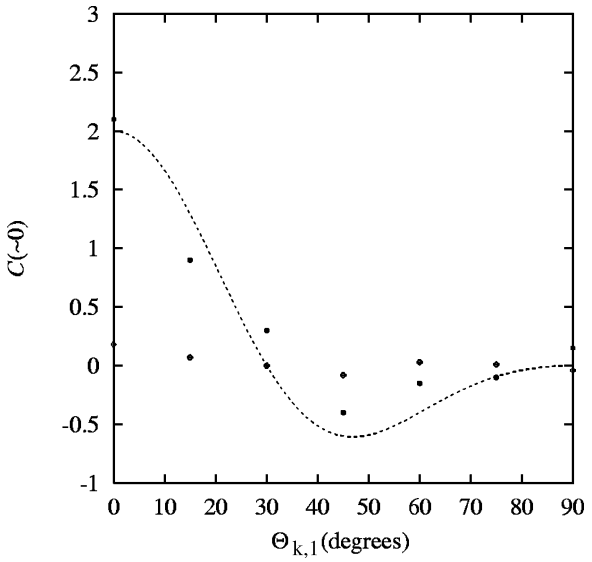

FIG. 8. The weighted mean value of $C(t)$ (parts per thousand) for $t=2$ to 20 plotted as a function of angle. The ● are from the ''fluctuating'' region, while ⊙ are from the ''quiet'' region. The fit corresponding to the ''fluctuating'' part involves both a dipole component and a quadrupole component: the dashed line is $0.000\,20[1+3\cos(2\Theta_{k,l})]+0.000\,40\cos(4\Theta_{k,l})[2+\cos(2\Theta_{k,l})]$. Within the uncertainty, the ''quiet'' part is flat.

CH2 and CH0 with a 600-ms sliding average. In the present case, the ''quiet'' state according to this comparison has spherical symmetry since the ratio is very close to being unity (rms deviation of order 1%, this is also the case for the intensity ratios CH1 to CH0 and CH3 to CH0). The signal excursions from average have also dropped to less than a quarter, showing that the fluctuations seen in the two channels are mostly in phase and related to radial fluctuations. For the more ''fluctuating'' part there are still relatively large excursions from unity (rms deviation ~10%). This part corresponds to a collapse into a distorted shape without any fixed spatial direction, as also shown by the cross correlations. In this context we would like to point out that a ''quiet'' state by no means excludes the presence of symmetry breaking, but such a state does require a preferred direction in space. This kind of state would also have no angular dependence associated with the cross correlations.

An interesting feature of Fig. 6 is the observation that the average light output in all channels is actually higher in the nonspherical case than in the spherical case. In multibubble sonoluminescence the light production is believed to be diminished if the collapse is nonspherical [44]. One would naturally have believed this to be the case also in the single bubble case since the energy focusing in the collapse will be more diffuse and the resulting temperature lower. As noted in Ref. [23], this has implications for the efficiency of sonoluminescing bubbles as chemical microreactors.

An explanation of the observation may be found in the wiggles in the equilibrium curve possibly resulting in multiple stable equilibria as suggested by Brenner *et al.* [45]. However, according to Ref. [46], where further damping mechanisms were introduced, it is unclear whether these multiple stable equilibria states do exist.

In Fig. 9 we see the time series for a bubble in a state that over the space of 50 s develops to show appreciable changes in the emission seen by the four channels. The data are from an earlier time series belonging to the same configuration (CH0, 0°; CH1, 15°; CH2, 60°; CH3, 90°) as used in Fig. 6, and likewise have been normalized with the average over all 47 hours. Furthermore, notice that the relative signal strengths are rather different (most notably, the signal in CH1 is always higher than those of CH2 and CH3). This could of course be construed as being a result of a translation in space from the average position of the bubble. From the distance squared law for the intensity of the emitted light, this would only require a shift of ~3 mm. However, this would mean that the bubble should move away from both fibers placed at 0° and 90°, while more or less stay at a constant distance from the two others that are spaced in between (notice especially the time track from the fiber placed at 15°, CH1), conditions that are obviously impossible to fulfil. This argument holds regardless of the normalization. Therefore, the most reasonable explanation is that we see the emission from a shape distorted bubble that is changing its preferred direction in space and possibly to some extent the degree of distortion.

This interpretation of the data would agree with the symmetry axis pointing in the direction of 10° (nearly in the direction of CH1) at the start of the time series and turning

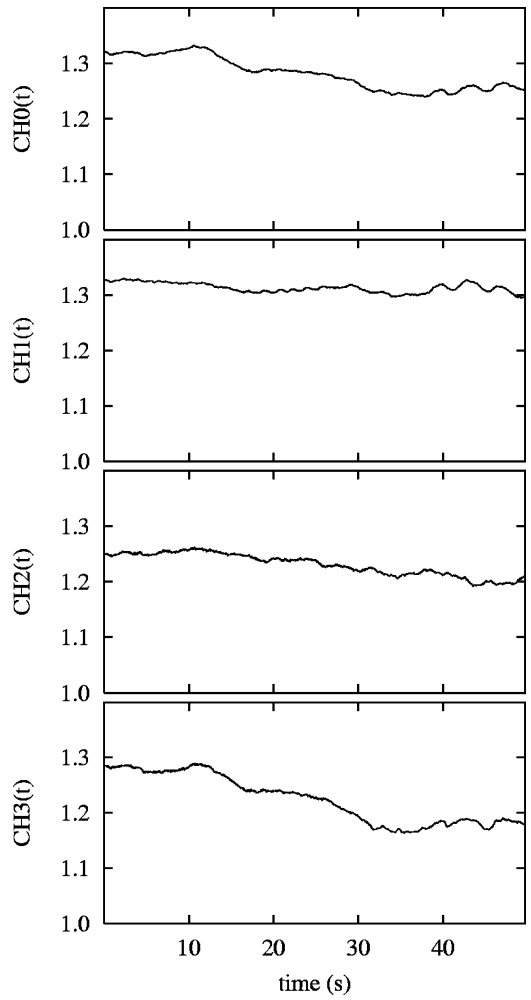

FIG. 9. Time series from a noisy state, which, with the passage of time, show a slow change in emission that can be associated with a change in direction and size of a shape distortion. Time average over 6 s.

some 20° in the direction of CH2 at the end. Of course we can only say something about the projection in the plane of the fibers. The bubble emission must furthermore include both dipole and quadrupole radiation.

Such observations easily lead to the notion that bubbles may exist in distorted states, where the symmetry axis may be precessing around a fixed direction in space. Such states will also give rise to an angular dependence for the cross correlation although no true integration over the entire space has been performed. Here we have to resort to looking at the autocorrelation too. For a true spatial integration to occur, these must be identical for all channels. This is a necessary but not sufficient condition and in the end a careful analysis of the time series themselves is also needed.

D. Spatial symmetry

The observation of states with quadrupolar radiation content, together with the observation of states with a stable preferred direction in space, where the cross correlation $C_{k,l}(0)=0(k\neq l)$, makes it virtually impossible to map out states using sequential positioning of two detectors. To obtain an even remotely efficient coverage of three dimensional space one needs detectors of order 16. In the present experiment we have settled on a practical limit of four giving six relative angles in the cases where a meaningful calculation of cross correlations can be performed.

In order to establish the symmetry of the problem we have investigated several different spatial configurations. The influence of spatial translation of the bubble is investigated with a configuration of all fibers in the horizontal plane of the bubble with this in the center and with two fibers opposing each other, i.e., fibers placed at 0°, 30°, 120°, and 180°. To get better spatial resolution we have employed a configuration with all fibers having relative angles less than or equal to 90°, i.e., fibers placed at 0°, 15°, 60°, and 90°. Finally, to look for anisotropy we have investigated a configuration with three fibers in the equatorial plane at relative positions 0°, 45°, 90°, and one directly below the bubble.

The analysis of data from long term stable time series belonging to the broad distribution of peak heights results in the following. The angular dependence of the cross correlation is seen to have a dominant 90° symmetry, thus, as already mentioned, displacement of the bubble in space is ruled out as causing the effect observed, as are the fluctuations in flash intensities of a spherical symmetric bubble. The effect of refraction of light by sound waves in water is, as pointed out in Ref. [18], too weak to be visible. The slight asymmetry present in some data could, though, be an indication of some translatory movement.

In all three cases the data can be fitted with various combinations of dipole and quadrupole radiation contents. Thus in these cases the bubble has no preferred orientation in space and there is no difference in the horizontal and the lateral behavior. Typical values of the change with angle of the cross correlation are of order 10 parts per thousand, although much higher values are occasionally observed.

E. Correlations over long offset times

The length of our time series allows us to calculate the autocorrelations and cross correlations out to rather large time differences, in fact, much longer than was possible for Weninger *et al.* [18] and with much better precision. An example of the cross correlation corresponding to a dipole state is shown in Fig. 10.

Several features stand out in this plot. The symmetry around 90° seen at zero offset time is nontrivially present out to very long offset times as the curves belonging to 30° and 150° are nearly coincident. As in Fig. 2 of Weninger *et al.* there is an initial decay. This decay was associated with the Q value of the driving sound field by the authors. The flow field in the fluid in the immediate neighborhood of the bubble was assumed to be coupled to the shape distortion of the bubble and the memory in the flow field was assumed to have the same time constant as the sound field. Therefore the correlations were assumed to decay on the same time scale as the sound field. However, as seen from the oscillations present in the correlations, correlations are present on time scales far beyond what can be expected from the above ar-

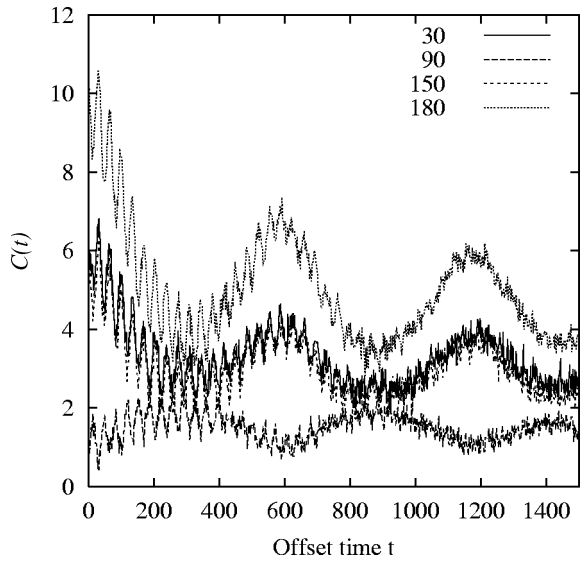

FIG. 10. Cross correlations (parts per thousand) as functions of offset time with interchannel angle as a parameter. Oscillations of length 35 cycles and 600 cycles are clearly present. Notice that the oscillations at 90° are in antiphase with the oscillations at 180° for both frequencies, so both must involve similar geometric shapes—only amplitude and frequency are different.

gument. Since the oscillations are seen in all channels (more or less prominently), they cannot be artifacts, but must originate in a real physical process. In most cases the oscillations are not occurring at a fixed frequency but rather belong to a narrow band of frequencies resulting in a beat observed in the correlations (see Fig. 11).

That the oscillations originate in the electronics is of course a possibility. However, this is highly unlikely in view of the observed symmetry properties (see Fig. 11 and comments above). Furthermore, the oscillations are also visible directly in the time series with phases linked to the positions of the fibers, regardless of the actual combination of the electronic connections.

Also in some cases two very different bands of frequencies are present as seen in Fig. 10. What exactly is causing these oscillations is not clear. Possibilities are either a slow pulsation or precession of the dipolar state, or combinations of these possibilities with a circular movement, as recently observed in various organic liquids [47]. An interesting possibility is the capture of a grain of dirt by the bubble and the following precession of the dirt around this [48]. However, the probability that all channels would be affected is very low and symmetry arguments also seem to exclude this as well as circular motion as explanations in most cases. The dirt particle could, however, trigger the bubble distortion, and then the frequencies would be linked to the motion of the dirt particle. Whatever the explanation, the simultaneous phase changes in the cross correlations, together with the progressive change for increasing angles, show the effect to be long lived (many seconds) and coupled to distortion of the spherical state (see also later discussion on period doubled states).

IV. PERIOD DOUBLING

Frequently time series showed that the light emission was period doubled [27]. Bifurcations are seen in all channels simultaneously, except in a few cases of a stable preferred direction where one fiber points towards a node. Cases with stable preferred directions in space will be treated in Sec. IV B. However, individual time tracks are, as mentioned above, rather confused. In the raw time series a sliding point average (of order 100 points or more) separately for odd and even times was necessary to observe the period doubling, and although this could be present for minutes at a time, the phase would slip. The measurements presented here are all performed without the use of filters. Thus, correlations are calculated according to Eq. (5). In Sec. IV A we shall concentrate on states with no preferred direction in space.

A. No preferred spatial direction

From the measurement of autocorrelations and cross correlations presented in Ref. [27] it was concluded that the period doubling was a geometric effect. While this conclusion cannot be disputed there are still open questions concerning features in the data and the interpretation of the cause. Presumably, the distortions involved are spherical harmonics ($n=2$). As already pointed out in Sec. III B, measurements by Weninger *et al.* using a two point angular correlation scheme suggested that an ellipsoidal bubble shape could result in a radiation field with dipolar content. In fact, our data fit rather well to a radiation field with dipolar and quadrupolar content (only dipolar content was used in the fit

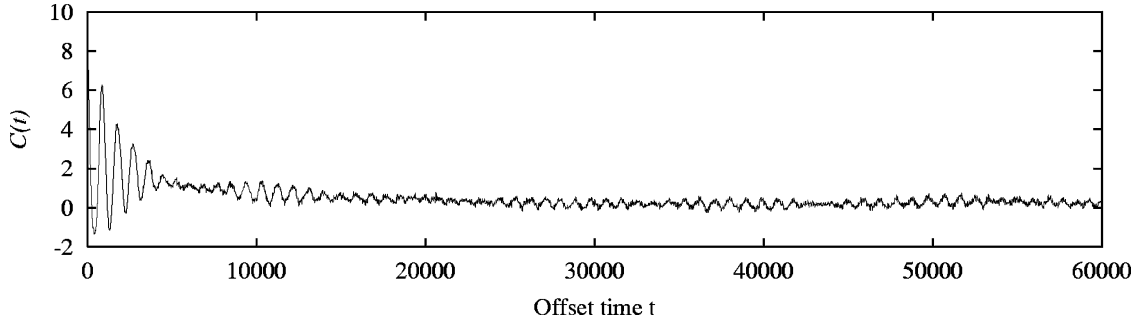

FIG. 11. Cross correlations (parts per thousand) as functions of offset time. Data are calculated from a 2-min time series. Only correlations between channels 180° apart are shown as representative of all. Notice oscillations and beat.

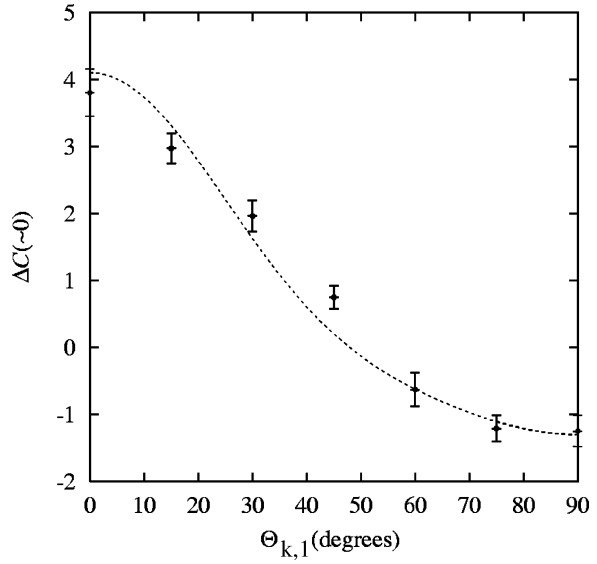

FIG. 12. The mean value of $\Delta C(t)$ (parts per thousand) for $t=2$ to 20 plotted as a function of angle. For the angle 0° the mean value of the autocorrelation from the four channels is used. The dashed line is $0.0008[1+3\cos(2\Theta_{k,l})]+0.0003\cos(4\Theta_{k,l})[2+\cos(2\Theta_{k,l})]$.

presented in Ref. [27]) as seen from Fig. 12. A reasonable assumption is therefore that the periode doubled state is a periodic shift between two different $n=2$ bubble shapes. The fit in Fig. 12 is given by the following expression for the correlation difference:

$$\Delta C_{k,l}(t\sim 0)=0.0008[1+3\cos(2\Theta_{k,l})]+0.0003\cos(4\Theta_{k,l})\times(2+\Theta_{k,l}), \quad (6)$$

where $\Delta C_{k,l}(t\sim 0)$ is defined as $\Delta C_{k,l}(t\sim 0)=C_{k,l}(t_{even})-C_{k,l}(t_{odd})$, i.e., the difference between small time correlations calculated for even and odd offset times separately.

Some features in the correlations were, however, not understood earlier. Careful inspection of the raw data files shows that the initial drop in the autocorrelations (Fig. 1 in Ref. [27]) were caused by short lived structures ($\sim$100 flashes) that occur once in a while in all channels but never in any two channels simultaneously. These structures (which elevate autocorrelations for $t\lesssim 50$) could possibly be related to the orbiting dust grains reported in Ref. [48]. Notice, however, that the sizes of the period doublings at offset times close to zero and at offset times around 50, where the drop has leveled off, are nearly identical. Thus these structures affect the normalization, and not the size of the period doubling. In the cross correlations the structures have no effect, since the angles between the fibers are too large for the peaks to be present in two different channels simultaneously. The presence of the peaks therefore has no effect on the graph of Fig. 12.

B. Stable spatial symmetry

In the previous sections we have mostly been concerned with no obviously preferred direction in space. In this section we present results showing that a distorted bubble can actually retain its sense of direction for times of order of minutes at least. This would be extremely hard to detect if the size of the distortion is independent of time so the flash intensity is constant (see, however, Figs. 6 and 9 and subsequent discussion).

However, if the distortion is pulsating or even period doubled or the axis is just rocking in time, the situation is much less difficult. Since the period doubled case is the easiest to analyze and understand, we shall proceed with this case.

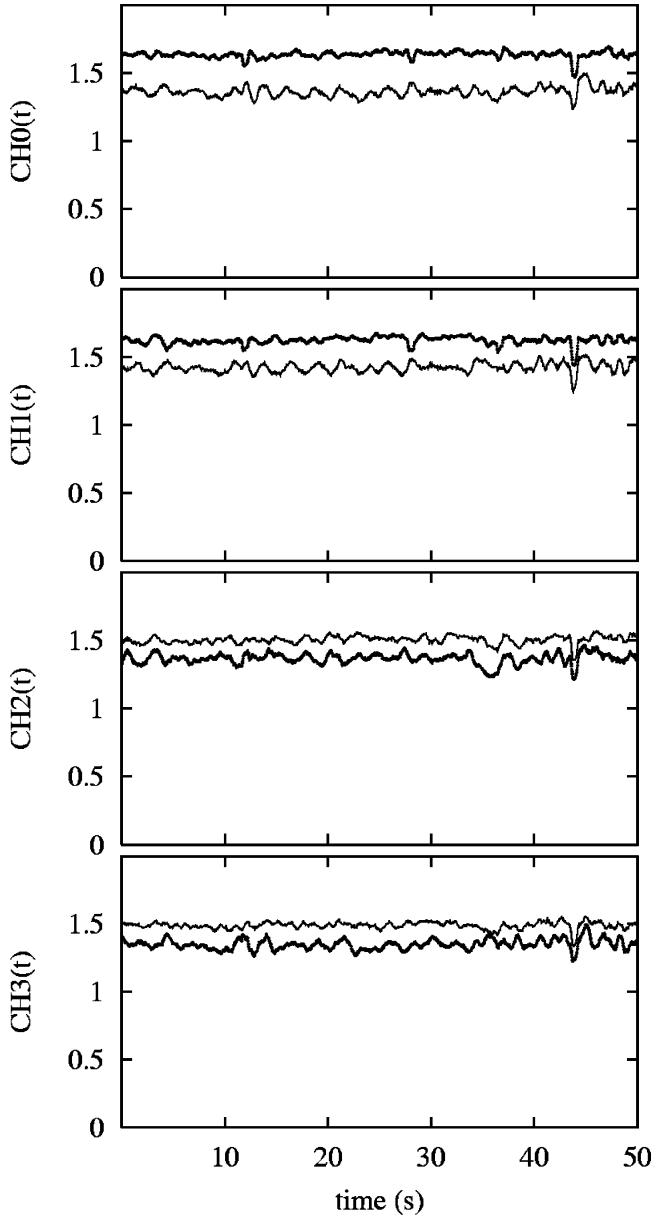

FIG. 13. Time series showing a normalized noisy signal in all four channels. The signals have undergone a sliding point average of 0.8 s for odd and even times separately to remove the statistical noise from the small count numbers per flash. Faster oscillations are also averaged out. Period doubling is clearly present, but also observable is the shape distortion as a size effect and phase shift.

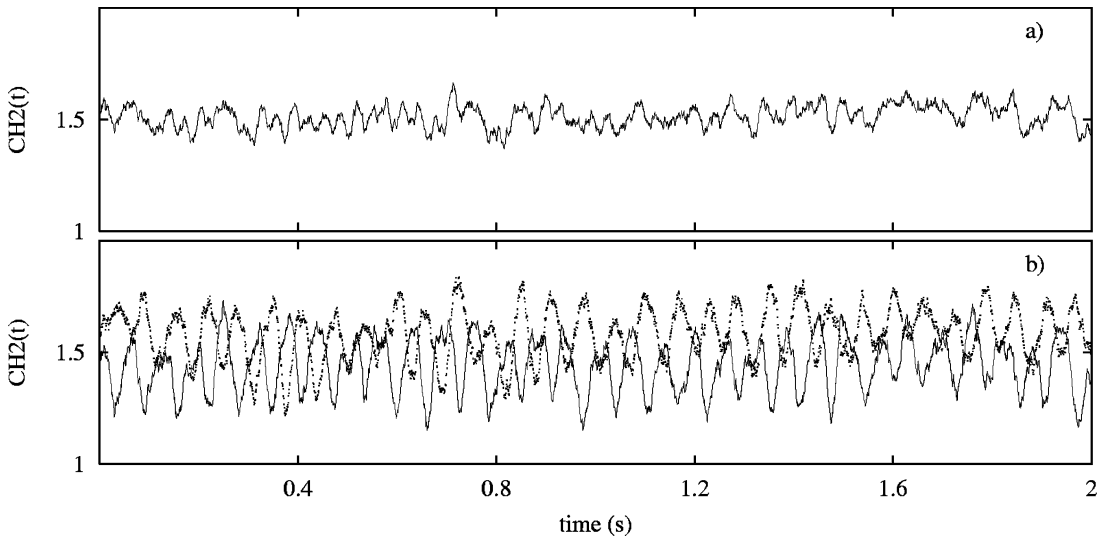

FIG. 14. Time series showing a noisy signal from CH0. In (a) the signals have undergone a sliding point average of 20 ms using all samples. In (b) the signals have undergone a sliding point average of 20 ms for odd and even times separately to remove the statistical noise from the small count numbers per flash. That period doubling is present is clearly observed in (b) while the narrow time signal in (a) has lost all traces of period doubling.

In Fig. 13 we display a 50-s-long time series where we have made a 0.8-s running average over even and odd times separately. (Fiber positions are CH0, 0°; CH1, 15°; CH2, 60°; CH3, 90°.) As seen, the time series split into two distinctly separate tracks. Thus we have period doubling. Furthermore, since, apart from fluctuations, even and odd time tracks for all channels are keeping the distance constant with time, either the period doubling is radial or the symmetry axis is fixed in space. That the latter is actually the case is seen by observing that the phase of the signals in channels CH0 and CH1 is opposite to that of channels CH2 and CH3. Also the size of the effect, normalized with the average signal size in the channel in question, is seen to be dependent on channel number with CH0 having a 20% difference and CH3 a 9% difference.

Unfortunately, four channels are not sufficient to map out the spatial intensity distribution when the deformation is stationary in space, but it is remarkable that the intensity (relative to the average intensity per channel) for, e.g., the even times is changing by an amount of no less than 30% with angle and that the maximum size of the period doubling is 20%.

In relation to the observation by Weninger *et al.* [18] on the ''fluctuating'' (''quiet'') states and their angular dependence, it is interesting to look at the signal strength distribution for the spatially stable period doubled state. In Fig. 14 we show a 2-s-long time series from CH2 (which is representative for all four channels) where in (a) we have made a 20-ms running average, while in (b) we have made a 20-ms running average over even and odd times separately. (The 20-ms sliding point average is close to the 10-ms binning used in Fig. 4 of Ref. [18]. A 2-s-long cut is displayed in order for the period doubling still to be visible with a 20-ms average.) In Fig. 15 we show the corresponding distributions. In Fig. 14(a) we see a rather quiet signal giving rise to the narrow distribution in the middle of Fig. 15. In Fig. 14(b) we see two distinct tracks with large fluctuations giving rise to the left and the right distribution peaks in Fig. 15.

Mostly we find that the lower intensity curve has larger ''fluctuations'' than the upper one for the same channel though occasionally this picture is inverted. Sometimes intensity fluctuations are in phase for the two tracks, at times in antiphase as in Fig. 14. These phenomena may be related to fluctuations in the direction of the symmetry axis or fluctuations in the bubble size or shape, especially if interference effects play a dominant role, although for all these possibili-

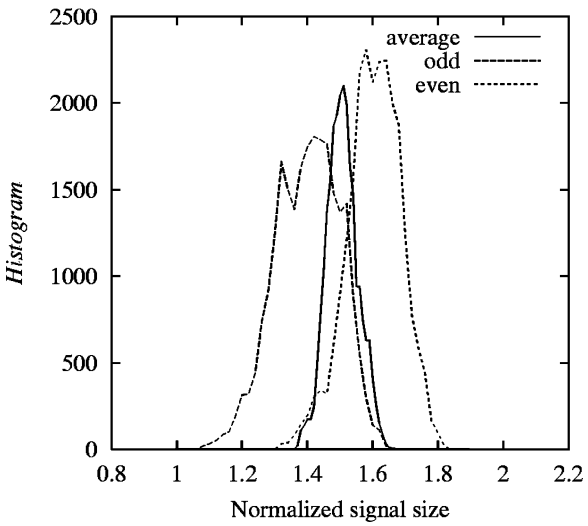

FIG. 15. The signal strength distribution belonging to CH0 of the time series displayed above in Fig. 14 using the same sliding point average of 20 ms to remove the statistical noise from the small count numbers per flash as above. The narrow distribution is from the sliding average over all samples, while the lower broader distribution is from the sliding average over the odd time samples and the upper peak from the sliding average over the even time samples.

ties, the resulting sign of the intensity change would depend on the angle between the symmetry axis and the direction to the observer. However, what becomes clear is that a ''quiet'' state may not be that different from a ''fluctuating'' state but can in reality be a distorted state, but with a stable symmetry axis in space or even a period doubled state, since none of these states will show an angular dependence in the correlations. With the length of the time series available (and due to the necessary statistical averaging) for Weninger *et al.* [18], a stable distorted state would have been impossible to detect and even a period doubled state would have been extremely difficult to observe. The results shown above do offer a plausible explanation, though, of why the time jitter is the same for the ''quiet'' (''fluctuation'') states and it would be interesting to see new results from an experiment combining the two types of measurements.

V. DISCUSSION

From the examples of bubble dynamics discussed in the previous sections, it is clear that stable SBSL in the sense of long lived states encompass myriads of possible states in time and space. To disentangle the precise nature of these states requires data from a much more complete coverage of three-dimensional space than we have presented. However, some features are emerging already from the four-channel experiment reported here.

From the knowledge acquired from the experimental results presented in this paper, it is clear that at least distorted states of shape $n=2$ (ellipsoids) are involved. From comparing the estimated values of $R_0 \sim 6$ μm and $P_A \sim 1.45$ bar with Fig. 2 from Ref. [23] the operating point in parameter space is above the parametric $n=2$ instability boundary. Thus it is reasonable to assume that the state excited is an $n=2$ state, where the growth of the amplitude is limited by nonlinear effects.

An obvious question to ask is what kind of states are the constituent states of the period doubling. The most likely guess on what goes on when the period doubling occurs is that two $n=2$ states of two different amplitudes are involved in the first bifurcation, four $n=2$ states of four different amplitudes are involved in the second bifurcation, and so on all the way to chaos.

The governing equation for the shape distortion is a Hill equation. For the parametric instability the driving term in the equation has the frequency of the external drive through its dependence on the time-dependent bubble radius $R(t)$ and its derivatives. However, the Hill equation is unstable towards half the frequency. Period doubling may hence be a consequence of this instability.

An open question is, whether the correlation measurement can tell anything about the mechanism giving light, the extent of the emitting region, and the opacity of the bubble. Weninger *et al.* [18] suggested that the angular dependence of the cross correlation in the small wavelength limit resulted from the refraction of the light pulse at the bubble surface, and that no dependence was seen in the long wavelength case due to the dominance of diffraction over refraction. However, various explanations of sonoluminescence suggest that surface radiation is present. Unless one assumes complete incoherence and the surface an ideal Lambertian diffuser for the light generated inside, surface radiation gives results that are nearly identical for not too large ellipticity. Note though that this argument assumes that no shadowing of surface areas is present. Thus for shape distortions with n even, e.g., a doughnut shape would give rise to multipole terms even under the above assumptions. For n odd the far field from a surface emitter as well as from a central emitter would be anisotropic but the cross correlation would not be symmetric around 90°, in contradiction to the symmetry observed in our experiments. One obvious problem in comparing with the hypothesis of refraction is the lacking knowledge of the actual refractive index inside the bubble. No conclusion can thus be reached on the question of the degree of opacity inside the bubble before the index of refraction inside the bubble at the time of emission is known, although certainly the strong compression of the gas in the bubble will increase the refractive index of the gas, thereby reducing the effect of light refraction.

However, it may still be useful to compare our measurements with the theoretical calculations of Ref. [19] that includes both refraction and diffraction effects. As mentioned, we observe fluctuations in the time series of order $\pm 30\%$ due to period doubling and zero angle cross correlations that reach up to 50 parts per thousand. A superficial comparison with Figs. 1 and 2 in Ref. [19] might lead to the conclusion that the bubbles in our experiments are strongly distorted. They also have to be rather large in order for the effect of refraction not to be quenched in the regime of red light. We would like to point out a discrepancy here. The effective wavelength of our ''red'' filter according to Fig. 2 is $\sim$610–630 nm, much further in the ''red'' and much sharper than the filter employed by Weninger *et al.* And even then we see an angular dependence for the red light. This suggests to us that interference effects play an important role also at this long wavelength.

Turning again to the period doubled states, the measurements described above indicate why period doubling seen directly in the emitted light has eluded observation for so long. First, to recognize period doubling in a tumbling or short lived state is extremely difficult without some kind of averaging where one explicitely looks for such a state. Second, one has to be in the right regime of parameters. Most of our observations of period doubling are in the regime of high gas content and high luminosity bubbles driven close to extinction. Third, to observe even a directionally stable long lived state without looking at correlations or averaging, one would need a detector catching about a thousand photons per glimpse to lift the period doubling out of the noise and even then the detector could accidentally be placed close to a node of the period doubled emission and the period doubling again be lost in the noise. However, the present experiment gets around these problems by using four detectors and statistics on very long time series.

VI. CONCLUSION

In conclusion, we have performed spatial and temporal correlation measurements on the light emission from a

sonoluminescing bubble using a four-channel fiber based detection system.

These measurements show that an immensely variable bubble dynamics is possible. We observe high luminosity states that have spherical symmetry, shape distorted states that have symmetry axes tumbling in space, shape distorted states that have a symmetry axis fixed in space or have a symmetry axis that precesses around a fixed direction in space, a direction that may even slowly precess itself. On top of this we also observe period doubled states. We have looked for evidence for higher period states and have some evidence for a second period doubling (i.e., period 4), but no odd period states have been seen.

The measurements show unequivocally that period doubling is a result of spontaneous breaking of spherical symmetry in the bubble collapse and is not seen in the light output per flash integrated over space. Thus we have observed period doubling in all the above mentioned cases except for the spherically symmetric case.

That the distorted states can survive for a very long time (hours) provides additional evidence that stable SBSL does not imply perfect spherical bubble collapse. The picture evolving is that the bubble first experiences excitation of a state of broken spherical symmetry (Refs. [17,18]) that is then subjected to a second (pitchfork) bifurcation into a period doubled state. Thus the explanation for these and previous observations [15–17] on period doubling and chaos should rather be sought in the three-dimensional Rayleigh-Plesset equation (see, e.g., Refs. [49,50] for a theoretical treatment of symmetry broken states) than in the symmetric radial Rayleigh-Plesset equation [28,29,34] that is essentially one-dimensional.

The governing equation for the shape distortion is a Hill equation. For the parametric instability the driving term in the equation has the frequency of the external drive and is thus unstable towards half this frequency. The observed period doubling in our experiment could very well be a consequence of this instability.

Another scenario is that a type of feedback or memory effect is involved. A likely candidate is that the distortion in shape is reflected in the velocity field of the surrounding fluid [51], but also the returning echo of the shock wave emitted into the water [34,35] from the previous bubble collapse may play a role as shown by a simulation on a simple model [52]. The latter mechanism may be linked to the actual geometry and physical properties of the system.

As for the light emission, the interference effect as calculated by Madrazo *et al.* [19] (although with smaller bubble sizes) seems to be a likely candidate for explaining the nonisotropic light emission. Interference effects with bubble sizes of order one or two wavelengths cannot only explain the observed dipole and quadrupole components but will probably fit our data even better, with the right choice of bubble size and ellipticity.

An interesting observation is that the total intensity from a shape distorted bubble may in fact be higher than the total intensity from a spherical bubble at the same external parameters (see Fig. 6). This could indicate that the bubble is perhaps subjected to an increased influx of air stabilizing a larger, maybe colder, bubble.

Finally, experiments that probe the connection between the timing of flashes and the degree of period doubling would be extremely interesting in view of previous results linking the two effects, especially since no period doubling was actually observed in the pulse heights directly but only in the timing in those experiments.

ACKNOWLEDGMENTS

The authors acknowledge financial support from the Danish National Science Foundation and the Carlsberg Foundation. We also wish to thank Gabor Simon and Peter Snoer Jensen for valuable discussions.

[1] D.F. Gaitan, L.A. Crum, R.A. Roy, and C.C. Church, J. Acoust. Soc. Am. **91**, 3166 (1992).
[2] D. F. Gaitan, Ph.D. thesis, University of Mississippi, 1990 (unpublished).
[3] Bradley P. Barber *et al.*, Phys. Rep. **281**, 65 (1997).
[4] S.J. Putterman and K.R. Weninger, Annu. Rev. Fluid Mech. **32**, 445 (2000).
[5] Dominic Hammer and Lothar Frommhold, J. Mod. Opt. **48**, 239 (2001).
[6] M.P. Brenner, S. Hilgenfeldt, and D. Lohse, Rev. Mod. Phys. **74**, 425 (2002).
[7] B.P. Barber and S.J. Putterman, Nature (London) **352**, 318 (1991).
[8] B. Gompf, R. Günther, G. Nick, R. Pecha, and W. Eisenmenger, Phys. Rev. Lett. **79**, 1405 (1997).
[9] R. Pecha, B. Gompf, G. Nick, Z.Q. Wang, and W. Eisenmenger, Phys. Rev. Lett. **81**, 717 (1998).
[10] M.J. Moran and D. Sweider, Phys. Rev. Lett. **80**, 4987 (1998).
[11] R.A. Hiller, S.J. Putterman, and B.P. Barber, Phys. Rev. Lett. **69**, 1182 (1992).
[12] R.A. Hiller, S.J. Putterman, and K.R. Weninger, Phys. Rev. Lett. **80**, 1090 (1998).
[13] T. Lepoint, D. De Pauw, F. Lepoint-Mullie, M. Goldman, and A. Goldman, J. Acoust. Soc. Am. **101**, 2012 (1997), and references therein.
[14] B.P. Barber, R.A. Hiller, K. Arisaka, H. Fetterman, and S.J. Putterman, J. Acoust. Soc. Am. **91**, 3061 (1992).
[15] R. Glynn Holt, D. Felipe Gaitan, Antony A. Atchley, and J. Holzfuas, Phys. Rev. Lett. **72**, 1376 (1994).
[16] Peter S. Jensen, M.Sc. thesis, Niels Bohr Institute/CATS, 1998 (unpublished).
[17] J.A. Ketterling and R.E. Apfel, Phys. Rev. E **61**, 3832 (2000).
[18] K. Weninger, S.J. Putterman, and B.P. Barber, Phys. Rev. E **54**, R2205 (1996).
[19] A. Madrazo, N. Garcia, and M. Nieto-Vesperinas, Phys. Rev. Lett. **80**, 4590 (1998).
[20] Y. Tian, J.A. Ketterling, and R.E. Apfel, J. Acoust. Soc. Am. **100**, 3976 (1996).
[21] E.H. Trinh, D.B. Thiessen, and R.G. Holt, J. Fluid Mech. **364**, 253 (1998).

[22] J.A. Ketterling and R.E. Apfel, J. Acoust. Soc. Am. **107**, L13 (2000).
[23] Hao Lin, Brian D. Storey, and Andrew J. Szeri, Phys. Fluids **14**, 2925 (2002).
[24] H. Lin, B.D. Storey, and A.J. Szeri, J. Fluid Mech. **452**, 145 (2002).
[25] B.D. Storey, Phys. Rev. E **64**, 017301 (2001).
[26] B.D. Storey and A.J. Szeri, Proc. R. Soc. London, Ser. A **456**, 1685 (2000).
[27] J.S. Dam, M.T. Levinsen, and M. Skogstad, Phys. Rev. Lett. **89**, 084303 (2002).
[28] Werner Lauterborn and Engelbert Suchla, Phys. Rev. Lett. **53**, 2304 (1984).
[29] Werner Lauterborn and Andreas Koch, Phys. Rev. A **35**, 1974 (1987).
[30] Joachim Holzfuss and Werner Lauterborn, Phys. Rev. A **39**, 2146 (1989).
[31] Lord Rayleigh, Philos. Mag. **34**, 94 (1917).
[32] M. Plesset, J. Appl. Mech. **16**, 277 (1949).
[33] Ritva Löfstedt, Bradley P. Barber, and Seth J. Putterman, Phys. Fluids A **5**, 2911 (1993).
[34] G. Simon, P. Cvitanović, M.T. Levinsen, I. Csabai, and Á. Horváth, Nonlinearity **15**, 25 (2002).
[35] J. Holzfuss, M. Rüggeberg, and R. Mettin, Phys. Rev. Lett. **81**, 1961 (1998).
[36] W. Moss, D. Clarke, and D. Young, Science **276**, 1398 (1997).
[37] N. Garcia, A. P Levanyuk, and V.V. Osipov, JETP Lett. **70**, 431 (1999).
[38] P. Mohanty and S.V. Khare, Phys. Rev. Lett. **80**, 189 (1998).
[39] M. Visser, S. Liberati, F. Belgiorno, and D.W. Sciama, Phys. Rev. Lett. **83**, 678 (1999).
[40] J.R. Willison, Phys. Rev. Lett. **81**, 5430 (1998).
[41] D. Tsiklauri, Phys. Rev. E **56**, R6245 (1997).
[42] G. Simon and M. T. Levinsen, Phys. Rev. E (to be published).
[43] Jeppe S. Dam, Mogens T. Levinsen, and Martin Skogstad (unpublished).
[44] B. Metten and W. Lauterborn, in *Nonlinear Acoustics at the Turn of the Millennium*, edited by Werner Lauterborn and Thomas Kurz, AIP Conf. Proc. No. 524 (AIP, Melville, NY, 2000), pp. 429–432; B. Metten, Ph.D. dissertation, University of Göttingen, 2000 (unpublished).
[45] M.P. Brenner, D. Lohse, D. Oxtoby, and T.F. Dupont, Phys. Rev. Lett. **76**, 1158 (1996).
[46] Y. Hao and A. Prosperetti, Phys. Fluids **11**, 2008 (1999)
[47] Yuri T. Didenko, William B. McNamara III, and Kenneth S. Suslick, Nature (London) **407**, 887 (2000).
[48] K.R. Weninger, P.G. Evans, and S.J. Putterman, Phys. Rev. E **61**, R1020 (2000).
[49] Y. Hao and A. Prosperetti, Phys. Fluids **11**, 1309 (1999); B.D. Storey, Phys. Rev. E **64**, 017301 (2001), and references therein.
[50] U.H. Augsdörfer, A.K. Evans, and D.P. Oxley, Phys. Rev. E **61**, 5278 (2001).
[51] A. Prosperetti, Q. Appl. Math. **34**, 339 (1977).
[52] M. T. Levinsen and G. Simon (unpublished).